Effect of B_2O_3 addition on structure of nepheline glass-ceramics for dental applications

Ali S. Alzahrani[1,*], Dominique de Ligny[2]

[1]*Department of Basic Medical, Oral and Allied Dental Sciences, College of Dentistry, Taif University, P.O. Box 11099, Taif, 21944, Saudi Arabia*

[2]*Department Department of Materials Science and Engineering, Friedrich-Alexander-Universität Erlangen-Nürnberg (FAU), Erlangen 91058, Germany*

Received 1 November 2025; received in revised form 12 February 2026; accepted 15 March 2026

Abstract

This study investigates the effect of substituting Al_2O_3 with B_2O_3 (0–4 mol%) in nepheline-based glasses intended for advanced dental applications. Differential scanning calorimetry, X-ray diffraction, Raman spectroscopy, dilatometry and scanning electron microscopy were used to examine the structural and thermal evolution of the modified compositions. Increasing B_2O_3 content decreased the glass transition and softening temperatures and suppressed nepheline crystallisation, leading to the enhanced amorphous stability. Raman analysis revealed progressive network depolymerisation due to the conversion of Al–O–Si linkages to BO_3 structural units, while dilatometry demonstrated improved thermal expansion compatibility with zirconia and metal substructures. SEM confirmed that higher B_2O_3 levels reduced crystal formation and yield smooth, homogeneous microstructures ideal for aesthetic dental applications. The results show that B_2O_3 contents of 2–3 mol% provide optimal thermal behaviour, translucency potential and structural uniformity, positioning these compositions as promising candidates for use in dental veneering porcelains, pressable glass-ceramics and CAD/CAM restorative materials.

***Keywords**: B_2O_3, nepheline, glass-ceramics, dental applications, crystallization*

I. Introduction

Glass-ceramics have gained significant attention in dentistry due to their unique combination of high strength, chemical durability and excellent aesthetic qualities [1–3]. Among them, nepheline-based glass-ceramics ($NaAlSiO_4$) are of particular interest because of their favourable mechanical properties, good biocompatibility and suitability for use as metal-free restorative materials [4–6]. Over the past decades, several studies have explored nepheline crystallisation in aluminosilicate glass systems, highlighting their potential for clinical applications ranging from crowns and bridges to minimally invasive restorations [7–9].

Despite these advantages, the practical use of nepheline glass-ceramics is hindered by their inherently high melting and processing temperatures [10,11]. These elevated thermal requirements not only increase manufacturing costs but also limit scalability and compatibility with modern processing routes, including sintering and computer-aided design/computer-aided manufacturing (CAD/CAM) techniques [12,13]. Consequently, there is a strong need to develop compositional modifications that can reduce the processing temperatures without compromising structural integrity and functional performance [14,15].

Boron oxide (B_2O_3) plays a significant role in glass systems as both a network former and an effective fluxing agent, depending on composition and modifier content. Structurally, boron is incorporated into the glass network in trigonal (BO_3) and tetrahedral (BO_4) coordination states, with the relative proportion governed by the presence of alkali or alkaline earth oxides. The predominance of BO_3 units introduces a more open and flexible network compared with purely silicate structures, thereby reducing melt viscosity and lowering the melting and softening temperatures. This behaviour gives boron-containing compositions strong fluxing characteristics, facilitating melting, homogenisation and forming at reduced thermal budgets. At the same time, partial conversion of BO_3 to BO_4 units in modified borate and borosilicate glasses enhances network connectivity and chemical

*Corresponding author: tel: +966556232688
e-mail: *asalzahrani@tu.edu.sa*

durability. Owing to this dual structural role, B_2O_3 is widely used to tailor processing temperature, thermal expansion and stability in advanced technical and dental glass and glass-ceramic materials [16–18]. Furthermore, B_2O_3 can influence the crystallisation, promote densification during sintering and potentially improve the balance between mechanical and thermal properties [19,20]. However, systematic studies on the effect of B_2O_3 additions in nepheline-based dental glass-ceramics remain limited, particularly in terms of correlating composition with crystallisation behaviour and processing performance.

The present study addresses this gap by investigating the role of B_2O_3 additions in nepheline glass-ceramics intended for dental applications. A series of compositions containing 0–4 mol% B_2O_3 were synthesised using the melt-quench technique and the resulting glasses and derived glass-ceramics were analysed using differential scanning calorimetry (DSC), X-ray diffraction (XRD), Raman spectroscopy, scanning electron microscopy (SEM) and dilatometry measurements. The objective is to clarify the influence of B_2O_3 on melting, crystallisation and sintering behaviours, and to evaluate its potential as a compositional modifier for improving the process-ability of nepheline-based dental glass-ceramics.

II. Experimental

2.1. Glass sample preparation

Table 1 presents the compositions of the parent glasses. The glasses were prepared using the conventional melt-quench technique. Boron trioxide (B_2O_3) was incorporated into the compositions by substituting aluminium oxide (Al_2O_3) in increments of 1 mol%. This approach yielded five distinct glass batches: one control composition without B_2O_3 and four compositions containing 1–4 mol% B_2O_3. The raw materials were of high purity: silicon oxide (SiO_2, 98%), aluminium oxide (Al_2O_3, 99.9%), sodium carbonate (Na_2CO_3, 99%), potassium carbonate (K_2CO_3), calcium carbonate ($CaCO_3$, 99%), lithium carbonate (Li_2CO_3, 98%) and boric acid (H_3BO_3, 99.8%). Each batch weighed 50 g and was dry-mixed thoroughly to ensure homogeneity prior to melting. Batches were held at 850 °C for 24 h to allow decomposition of the carbonate precursors before heating to the melting temperature. The mixtures were melted in a platinum crucible using an electric furnace at range 1550–1600 °C for 3 h. Part of the glass was cast into a graphite mould to obtain bulk specimens for dilatometry analysis, while the remaining melt was quenched in water to produce glass frits. The cast glasses were immediately transferred to a preheated annealing furnace for annealing at 450 °C for 2 h and then allowed to cool gradually to room temperature overnight. The glass frits were milled individually into fine powders using an MG2000 autogrinder from POWTEQ at a pressure level of 4 and a speed of 80 rpm, for 40 min with utilisation of isopropanol to minimise the formation of dust. The milled glasses were sieved for 45 min through a stainless-steel sieve with a mesh size of 125 μm. The collected fraction (≤125 μm) was analysed by laser light scattering (LA960, Horiba). For each composition, five measurements were performed and the average particle size (D_{50}) was found to be in the range of 22–35 μm, which is consistent with the particle size typically used for layering dental porcelain [22].

Table 1. Starting glass compositions in mol% and ICP results

Glass Code	SiO_2	Al_2O_3	Na_2O	K_2O	Li_2O	CaO	TiO_2	B_2O_3	Total
B_2O_3 free	60	18	15	4	1	1	1	0	100.00
ICP [mol.%]	59.61	18.72	14.55	3.83	1.15	1.07	1.08	0	100.01
ICP [wt.%]	51.24	27.31	12.9	5.17	0.49	0.86	1.24	<0,01	100.21
1% B_2O_3	60	17	15	4	1	1	1	1	100.00
ICP [mol.%]	60.02	17.08	15.1	3.97	0.99	1.05	0.93	0.87	100.01
ICP [wt.%]	51.6	24.92	13.4	5.36	0.42	0.84	1.07	0.87	98.48
2% B_2O_3	60	16	15	4	1	1	1	2	100.00
ICP [mol.%]	59.83	15.78	15.02	4	1.02	1.04	1.22	2.09	100.00
ICP [wt.%]	52.22	23.36	13.52	5.48	0.44	0.85	1.41	2.11	99.39
3% B_2O_3	60	15	15	4	1	1	1	3	100.00
ICP [mol.%]	59.89	16.01	14.74	4.09	1.04	1.01	1.34	1.89	100.01
ICP [wt.%]	52.2	23.66	13.25	5.59	0.45	0.83	1.55	1.9	99.43
4% B_2O_3	60	14	15	4	1	1	1	4	100.00
ICP [mol.%]	60.17	14.44	14.81	3.64	1.23	1.02	1.12	3.04	99.47
ICP [wt.%]	53.46	21.57	13.45	5.02	0.54	0.84	1.32	3.1	99.30

2.2. Crystallisation of glass

Glass-ceramic specimens in the form of discs and rods were prepared by wet compaction of the glass powders (D_{50} = 22–35 μm). Each disc was produced from approximately one grams of glass powder mixed with 0.25 ml of deionised water. Excess moisture was removed using absorbent tissue. The resulting slurry was transferred into stainless-steel moulds with dimensions of 16 mm in diameter and 50 mm depth, for the discs shaped samples. The powders were compacted at 1 bar for 1 min and any remaining surface moisture was again removed prior to heat treatment.

Crystallisation by heat treatment in air - The green bodies were removed from the moulds and placed in a furnace (Bego Miditherm 200 MP, Germany) for crystallisation. The compacted powders from all five compositions (B_2O_3-free, 1, 2, 3 and 4 mol% B_2O_3) were treated simultaneously under identical conditions in air. Heat treatment was performed at 875 °C (±5 °C) for 1 h, using a heating rate of 40 °C/min, starting and finishing at 400 °C. The samples were cooled at a rate of 1 °C/min. This process converted the parent glasses into glass-ceramics. Heat treatment in air was performed to establish a baseline crystallization for all compositions and to evaluate the role of B_2O_3 under conventional conditions.

Crystallisation and sintering under vacuum - In parallel, a second group of specimens underwent sintering-crystallisation in a dental furnace equipped with vacuum capability (VITA VACUMAT 6000 M, Germany). The compacted powders from all five compositions were subjected to a heating rate of 40 °C/min, followed by a 1 min dwell at the sintering-crystallisation temperatures specific to each composition: 1075, 950, 900, 850 and 800 °C (each within ±5 °C) for the samples containing 0, 1, 2, 3 and 4 mol% B_2O_3, respectively. The starting and finishing temperatures were 400 °C and the cooling rate was maintained at 1 °C/min. Sintering-crystallisation under vacuum was employed to replicate dental processing conditions and to assess the suitability of the materials for porcelain-fused workflows commonly used in restorative dentistry. The sinterability of the glass powders under vacuum was assessed visually according to the following criteria: i) specimen edges should retain their shape without deformation, ii) surfaces should display a glossy appearance, iii) linear shrinkage should be reduced compared to the green compact, iv) surfaces should be free of visible porosity and v) specimens should exhibit translucency when observed against daylight.

2.3. Sample characterisation

The thermal behaviour of each glass powder (D_{50} = 22–35 μm) was investigated by differential scanning calorimetry (DSC, Netzsch, Germany). The DSC was operated at heating rates of 40 °C/min to simulate heating rate applied during sintering cycles in dental furnaces and Al_2O_3 was used as a reference material. Each run was performed on a 10 mg (±0.5) sample in a Pt-Rh crucible. The measurements were made in the temperature range from 25 °C up to a maximum temperature of 1400 °C.

Phase identification of the crystallised samples was carried out by XRD (Cu Kα radiation, 2θ range 10–80°) with a step size of 0.02° (D8 Advance XRD, Bruker). The crystalline phases were identified by comparison with reference patterns in the ICDD database using the Match! Software.

Structural analysis of the glass and glass-ceramic samples was performed using Raman spectroscopy at spectral range: 200–1400 cm^{-1}. Spectra were collected and averaged over three measurements per sample in a WITEC® manufactured set-up consisting of a laser (P_0 < 150 mW; λ = 532 nm), an alpha 300R microscope and the UHTS 300 spectroscope.

Dilatometry was performed on rectangular glass bars using a differential dilatometer (DIL 402PC, Netzsch, Germany). For each composition, two specimens were prepared, one cast glass and another specimen sintered-crystallised with 1 min hold glass-ceramics. The samples were heated from 25 to 1200 °C, or up to their softening point, at 3 °C/min under flowing nitrogen (1 ml/min). The NETZSCH Proteus 402PC software was used to extract dilatometric softening point (T_g) and coefficient of thermal expansion (CTE). CTE values were calculated between 100–400 °C and 100–500 °C.

The heat-treated samples (1 h) and the sintered-crystallized glass-ceramic specimens (1 min) were mounted in epoxy resin, then ground and polished to obtain flat surfaces. The polished surfaces were etched with 0.5 vol.% hydrofluoric acid (HF) for 10 s to partially dissolve the residual glassy phase and enhance phase contrast. To prevent surface charging, all specimens were sputter-coated with a thin layer of gold. Microstructural observations were performed using a field emission scanning electron microscope operated at an accelerating voltage of 5–20 kV. Images were collected at ×15,000 magnifications to evaluate crystallite morphology, size, and distribution.

Glass compositions were determined using inductively coupled plasma (ICP) spectroscopy following acid digestion. Samples were cleaned, dried, and ground to a fine powder. Approximately 50–100 mg of each sample was digested in a mixture of concentrated HNO_3 and HF. Elemental calibration was performed using multi-element standard solutions with appropriate blanks and internal standards. Measurements were conducted under standard instrument operating conditions, and each sample was analysed. Element concentrations were calculated

from calibration curves and reported as oxide weight percentages after applying dilution factors.

III. Results and discussion

The development of high-performance dental glass-ceramics requires precise control over microstructure, crystallisation kinetics and thermal behaviour in order to achieve high translucency, mechanical reliability and compatibility with restorative workflows such as CAD/CAM milling, veneering and pressable ceramic processing. Nepheline-based glasses are widely used in different applications due to their favourable optical and chemical strengthening properties; however, high melting and processing temperatures can compromise their application as dental restorative materials. In this context, the use of B_2O_3 as a structural modifier offers a promising pathway to reduce melting and processing temperatures and open the potential of nepheline-containing dental glass systems.

The ICP compositional analysis (Table 1) confirms good overall agreement between the nominal batch compositions and the measured glass compositions for all formulations. Major network formers (SiO_2, Al_2O_3) and modifier oxides (Na_2O, K_2O, CaO) remain close to their target values, with only minor deviations attributable to the melting and volatilisation effects. A systematic decrease in measured Al_2O_3 content and corresponding increase in B_2O_3 content is observed across the substitution series, confirming successful compositional control of the $Al_2O_3 \rightarrow B_2O_3$ replacement strategy. Slight variations in alkali oxides, particularly Li_2O and Na_2O, are consistent with their higher volatility at melting temperatures. The total oxide sums remain close to 100% in both mol% and wt.% analyses, indicating good chemical homogeneity and reliability of the melting and quenching procedures.

The substitution of B_2O_3 for Al_2O_3 significantly alters the connectivity of the silicate network. DSC analysis (Fig. 1) demonstrates that the increasing of B_2O_3 content leads to a reduction of about 152 °C in the glass transition temperature giving T_g: 713, 675, 639, 622 and 561 °C for the five glasses prepared with 0, 1, 2, 3 and 4 mol% B_2O_3, respectively. This behaviour indicates that boron reduces network rigidity by transforming tetrahedral AlO_4 units into BO_3 groups, producing a more depolymerised network [16]. For dental applications, a lower T_g and softening point provide considerable advantages during porcelain firing, CAD/CAM block crystallisation and pressable ceramic processing [23]. Lower firing temperatures minimise thermal stresses on zirconia or metal frameworks, reduce the risk of veneer chipping and improve dimensional stability during sintering [24]. Furthermore, the suppression of crystallization peaks in the DSC is particularly interesting in these glasses and in similar multicomponent glass systems containing mixed alkalis [25], which show more complex changes in many properties.

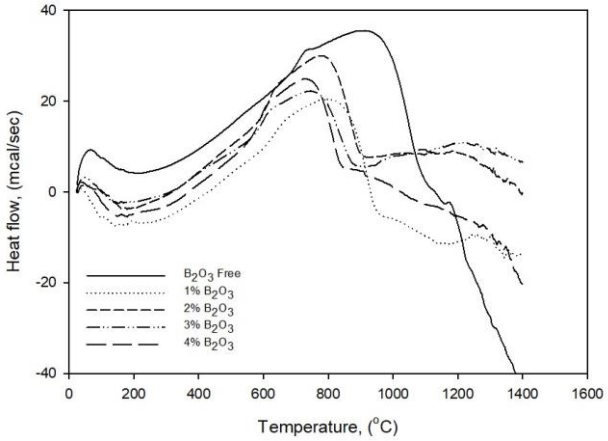

Figure 1. DSC curves of the prepared glasses with particle size <125 µm, at heating rate 40 °C/min, showing systematic decrease in heat flow as a result of Al_2O_3 substitution with B_2O_3

In glasses containing mixed alkali oxides (such as Na_2O-K_2O or Li_2O-Na_2O at constant total modifier content), the mixed-alkali effect produces a non-linear structural and thermal response that extends beyond simple network depolymerisation. At the atomic scale, different alkali cations possess distinct ionic radii and field strengths, which generate energetically unfavourable site mismatches within modifier-rich regions. Rather than sharing equivalent charge-compensating positions near non-bridging oxygens, each alkali species preferentially stabilises its own local coordination environment and enhances structural heterogeneity. This reduces cation mobility and alters the distribution and clustering of non-bridging oxygens without necessarily changing their total concentration. From a thermal analysis perspective, DSC curves reflect these effects through shifts in T_g, frequently accompanied by transition broadening that indicates a wider distribution of relaxation times. Enthalpy relaxation endotherms often become more pronounced, while crystallisation exotherms shift to higher temperatures and broaden because diffusion-controlled nucleation and growth are kinetically hindered [26,27]. The DSC results support the view that mixing alkalis in aluminosilicate glass systems hinders crystallisation [28]. Due to the lack of clear DSC crystallisation exotherms in this glass series, the effect of powder surface area and crystallization activation energy could not be determined.

XRD patterns (Fig. 2) confirm the reduction of nepheline crystallisation temperature with increasing B_2O_3 in both heat-treatment methods: at 875 °C for 1 h

in air and 1 min hold in a dental sintering furnace at the assumed sintering temperatures of 1075, 950, 900, 850 and 800 °C for the five glasses from B_2O_3-free to 4% B_2O_3, respectively. The disappearance of sharp nepheline reflections at higher substitution levels (>3% B_2O_3) indicates that the glass remains predominantly amorphous during controlled heat treatments. This is highly desirable in dental applications, where translucency and smooth microstructures are essential for achieving natural tooth-like optical behaviour. Amorphous structures scatter less light and produce more uniform shade distribution, enhancing the lifelike appearance of veneers, crowns and aesthetic CAD/CAM restorations [29].

Leucite ($KAlSi_2O_6$) is a rock-forming mineral related to zeolites and forms trapezohedral crystals [30]. It is found to develop alongside nepheline after heat treatment at 875 °C for 1 h in three samples (B_2O_3-free, 1%, and 2%), similar to those reported in the literature [31]. The Crystallography open database (COD) reference files were used to identify the developed crystalline phase; 96-901-3315 for nepheline and 96-901-3188 for leucite.

XRD patterns also demonstrate a systematic suppression of nepheline crystallisation with increasing B_2O_3 content under both thermal schedules, indicating that boron oxide significantly modifies crystallization kinetics and phase selection pathways of this glass system. Beyond a simple dilution effect, B_2O_3 alters the short- and medium-range order of the aluminosilicate network through the formation of BO_3 and BO_4 structural units, which compete with AlO_4 tetrahedra for charge compensation and disrupt the long-range ordering required for nepheline nucleation. Since nepheline ($NaAlSiO_4$) crystallisation depends on a locally ordered Na–Al–Si framework, the incorporation of borate species reduces structural similarity between the parent glass and the crystalline phase, thereby increasing the interfacial energy barrier for nucleation and lowering crystal growth rates [19]. This is consistent with the observed reduction in diffraction peak intensity and eventual disappearance of nepheline reflections at B_2O_3 levels above ~3%, where only a broad amorphous halo remains.

Peak broadening and intensity reduction in the residual crystalline reflections at intermediate B_2O_3 contents (2 to 3%) further suggest decreased crystallite size and/or reduced crystalline volume fraction rather than complete phase elimination, implying that boron primarily retards crystal growth before fully suppressing nucleation at higher substitution levels. The effect is observed under both prolonged heat treatment (875 °C, 1 h) and rapid dental firing cycles, indicating that boron increases kinetic stability across both diffusion-controlled and short-time sintering regimes.

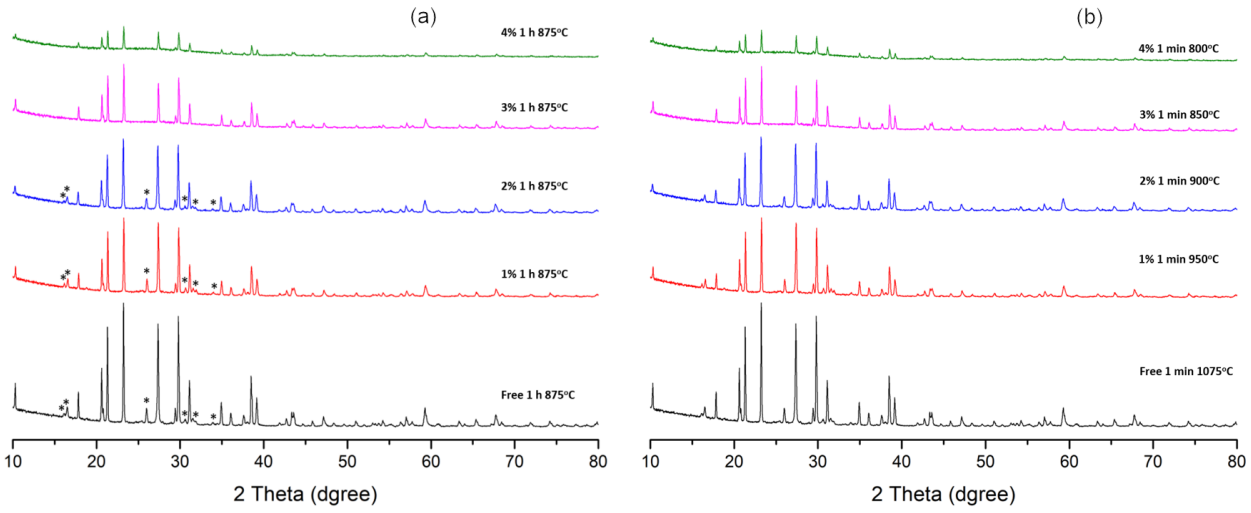

Figure 2. XRD patterns of the glass-ceramics showing developed crystalline phases: hexagonal nepheline ($NaAlSiO_4$) and nepheline-leucite (*) after: a) heat treatment at 875 °C for 1 h and b) sintering at selected temperature for 1 min

The concurrent appearance of leucite ($KAlSi_2O_6$) in low-boron compositions after extended heat treatment suggests a competitive crystallisation pathway controlled by alkali partitioning and local compositional fluctuations. Because leucite formation requires K-rich domains, while nepheline favours Na-rich aluminosilicate ordering, the reduction of nepheline intensity with increasing B_2O_3 may also reflect modifier redistribution and decreased alkali clustering in the boron-containing networks. Boron is known to reduce alkali mobility and modify charge-balancing relationships, which can suppress phase-separation precursors that often act as nucleation sites for feldspathoid phases [32]. The absence of leucite and nepheline peaks at higher B_2O_3 levels therefore indicates improved compositional homogeneity and reduced medium-range ordering tendencies, consistent with a more polymerised glass network.

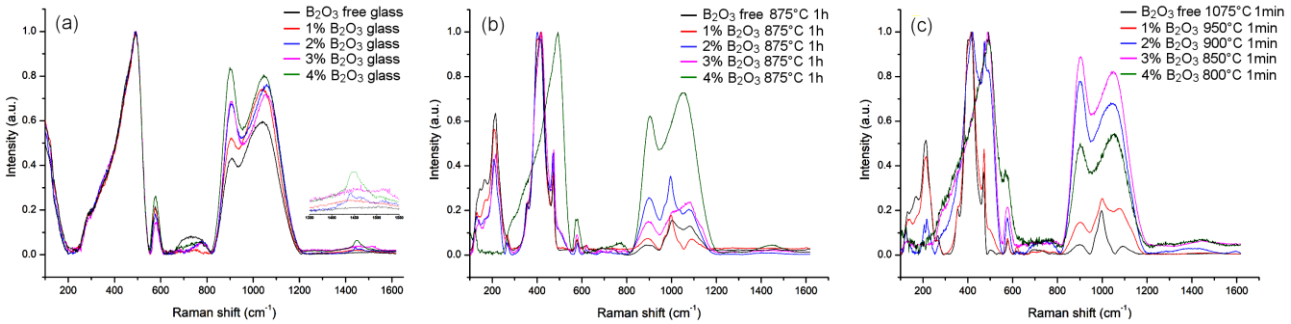

Figure 3. Raman spectra of: a) five base glasses, b) heat treated glasses at identical temperature 875 °C for 1 h and c) sintered glasses at selected temperature for 1 min

Raman spectra (Fig. 3) revealed systematic structural evolution as a function of both B_2O_3 content and heat-treatment schedule, providing complementary insight to the XRD and DSC results. In the as-quenched glasses (Fig. 3a), all compositions exhibit broad vibrational envelopes typical of amorphous aluminosilicate networks, with dominant bands near ~450–500 cm^{-1} (tetrahedral bending modes) and ~850–1100 cm^{-1} (Si–O–T stretching, T = Si, Al). With increasing B_2O_3 content, a gradual increase in intensity in the ~560–620 cm^{-1} region and a weak broad band above ~1350 cm^{-1} are observed, consistent with borate vibrational contributions from BO_3/BO_4 units [33]. These trends confirm that boron is structurally incorporated into the glass network and modifies structural connectivity. The stretching region simultaneously shows redistribution and partial shifting of the Q^n units, indicating boron-driven reorganisation of charge compensation and non-bridging oxygen distribution.

After prolonged heat treatment at 875 °C for 1 h (Fig. 3b), the Raman spectra show clear composition-dependent crystallisation behaviour. Low-boron glasses develop sharp, narrow bands in the 150–300 cm^{-1} lattice-mode region and partially resolved peaks in the tetrahedral stretching region, consistent with the formation of ordered aluminosilicate crystalline phases such as nepheline and leucite [34]. The bending region (~450–520 cm^{-1}) correspondingly sharpens, indicating increased framework periodicity. In contrast, glasses containing ≥3 mol% B_2O_3 retain broader bands and reduced intensity, demonstrating that long-range ordering is strongly suppressed [35]. The persistence of broad borate-associated bands confirms that boron remains incorporated within a residual glassy matrix. These spectral features indicate that B_2O_3 increases disorder and reduces structural similarity between the parent glass and the feldspathoid (nepheline-leucite) crystal structures, thereby raising nucleation barriers and slowing crystal growth, in agreement with the reduced crystalline peak intensity observed by XRD.

Raman spectra of the samples obtained after rapid 1 min firing (Fig. 3c) at composition-dependent temperatures show intermediate behaviour between the as-quenched and long-duration heat-treated states, highlighting the kinetic dimension of the crystallisation process. The boron-free composition treated at the highest temperature exhibits emerging lattice-mode peaks and partial stretching-band splitting, indicating rapid short-time ordering. However, peak widths remain broader than in the samples heat-treated at 875 °C for 1 h, consistent with limited crystal size and incomplete structural periodicity. As B_2O_3 content increases and firing temperature decreases, these crystalline signatures weaken progressively and the spectra revert toward glass-like envelopes. The stretching region remains intense but structurally broadened, indicating preserved tetrahedral connectivity with reduced long-range order. This demonstrates that boron addition suppresses not only equilibrium crystallisation, but also rapid kinetic ordering during short dental firing cycles.

Across all three thermal states, the Raman results consistently show that increasing B_2O_3 content promotes structural heterogeneity at the medium-range scale and redistributes tetrahedral environments, which collectively disrupt alkali-aluminosilicate ordering pathways required for nepheline and leucite formation. Spectroscopically, this is expressed as the persistence of band broadness, reduced lattice-mode intensity and enhanced borate vibrational contributions. The agreement between Raman disorder signatures, DSC crystallisation peak suppression and XRD phase reduction provides evidence that B_2O_3 acts as both structural and kinetic crystallisation inhibitor. From a processing perspective, this behaviour is highly beneficial for dental glass and glass-ceramic systems, as it widens the safe firing window, limits unwanted feldspathoid crystallisation and helps preserve optical homogeneity and thermal compatibility [36–39].

The dilatometric curves demonstrate a systematic evolution of thermomechanical response (Figs. 4 and 5, Table 2) with increasing B_2O_3 content and with conversion from parent glass to glass-ceramics (GC). In the linear expansion region (Fig. 4a), all parent glasses show near-parallel slopes up to the transition range, indicating broadly similar average bond

stiffness at low temperature. Only modest variation in slope is observed from 0–3 mol% B_2O_3, while the 4 mol% B_2O_3 composition exhibits slightly higher expansion, consistent with increased network flexibility due to greater borate participation and modified charge-compensation topology.

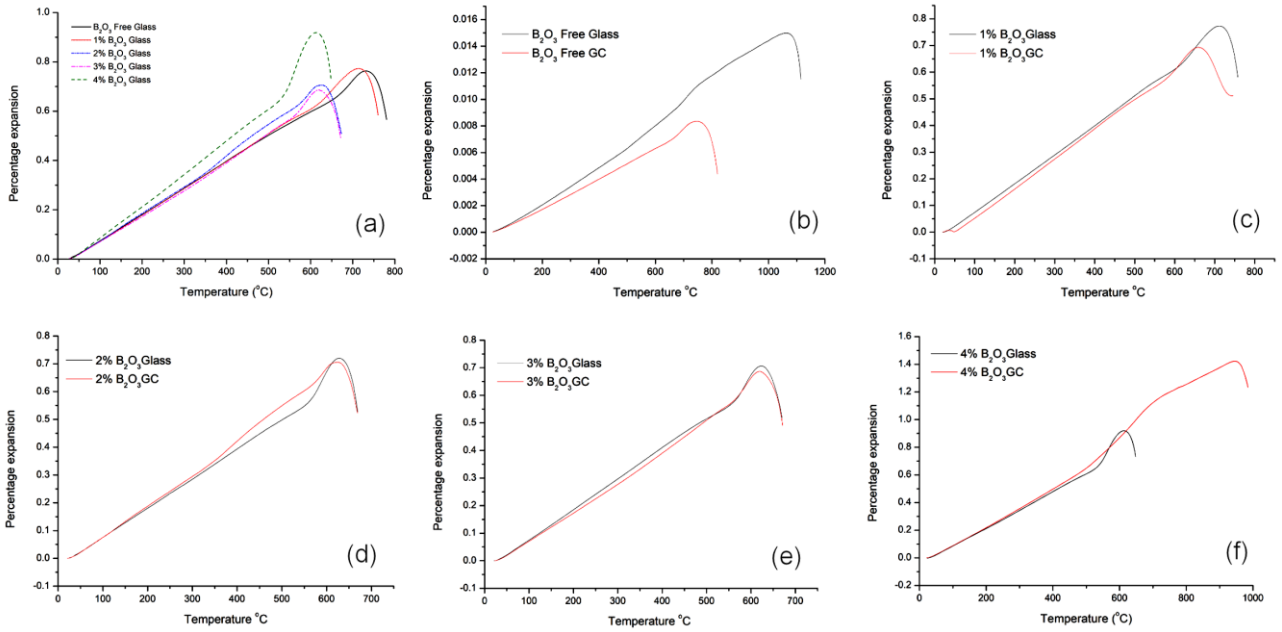

Figure 4. Dilatometric curves illustrating the changes in T_s and T_g and in CTE for: a) the five glasses as a result of substituting Al_2O_3 with B_2O_3 and changes before and after sintering-crystallisation for 1 min in dental furnace of samples with different B_2O_3 contents: b) 0, c) 1, d) 2, e) 3 and f) 4 mol%

Table 2. Properties of the glasses and sintered-crystallised glass-ceramics from DSC and dilatometry analysis

Glass code	T_g [°C] glass (DSC)	T_g [°C] glass (DIL)	T_g [°C] GC (DIL)	T_s [°C] onset glass (DIL)	T_s [°C] onset GC (DIL)	CTE ×10^{-6} glass		CTE ×10^{-6} GC	
						100-400 °C	100-500 °C	100-400 °C	100-500 °C
B_2O_3 free	713	669	638	731	1025	10.77	10.71	12.60	12.71
1% B_2O_3	675	621	608	712	945	10.82	10.93	13.66	14.01
2% B_2O_3	639	579	564	626	628	11.53	11.84	10.60	10.57
3% B_2O_3	622	568	564	622	623	10.64	10.96	11.12	11.01
4% B_2O_3	561	541	545	594	607	10.41	10.41	10.84	10.66

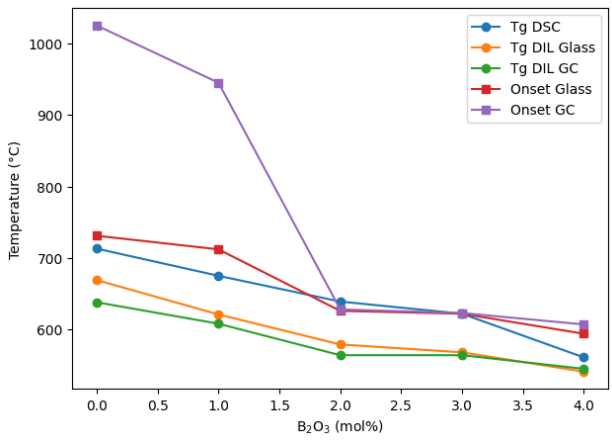

Figure 5. Thermal parameters versus B_2O_3 content for the studied glasses and corresponding glass-ceramics, showing glass transition temperatures from DSC and dilatometry and the dilatometric deformation onset

The glass transition region broadens progressively with increasing B_2O_3 content in both glass and GC curves. Instead of a sharp break in slope, higher-boron compositions show a more gradual curvature change, indicating a broader distribution of structural relaxation times. This behaviour possibly reflects increased medium-range structural heterogeneity introduced by mixed BO_3/BO_4 units and altered alkali charge-balancing environments, consistent with Raman band broadening and DSC T_g-region widening.

Clear crystallisation-related dimensional effects are visible when comparing glass vs. glass-ceramics curves. In the B_2O_3-free composition (Fig. 4b), the GC curve shows markedly lower total expansion and earlier deviation from the glass curve, followed by contraction near the deformation peak. This is a classic signature of significant nepheline crystallisation [6] and aligns with the XRD identification of nepheline formation. At 1 mol% B_2O_3 (Fig. 4c), the separation between the glass and GC curves remains evident but reduced. This indicates a lower crystalline fraction and/or finer crystal dispersion. At 2 mol% B_2O_3 (Fig.

4d), the glass and GC curves are very similar over most of the temperature range, changing only near the softening temperature (T_s). At 3 mol% B_2O_3 (Fig. 4e), the curves nearly overlap, indicating minimal crystallization-induced shrinkage. At 4 mol% B_2O_3 (Fig. 4f), the GC curve shows greater high-temperature expansion and extended deformation range, indicating very limited crystallisation and a more residual matrix response.

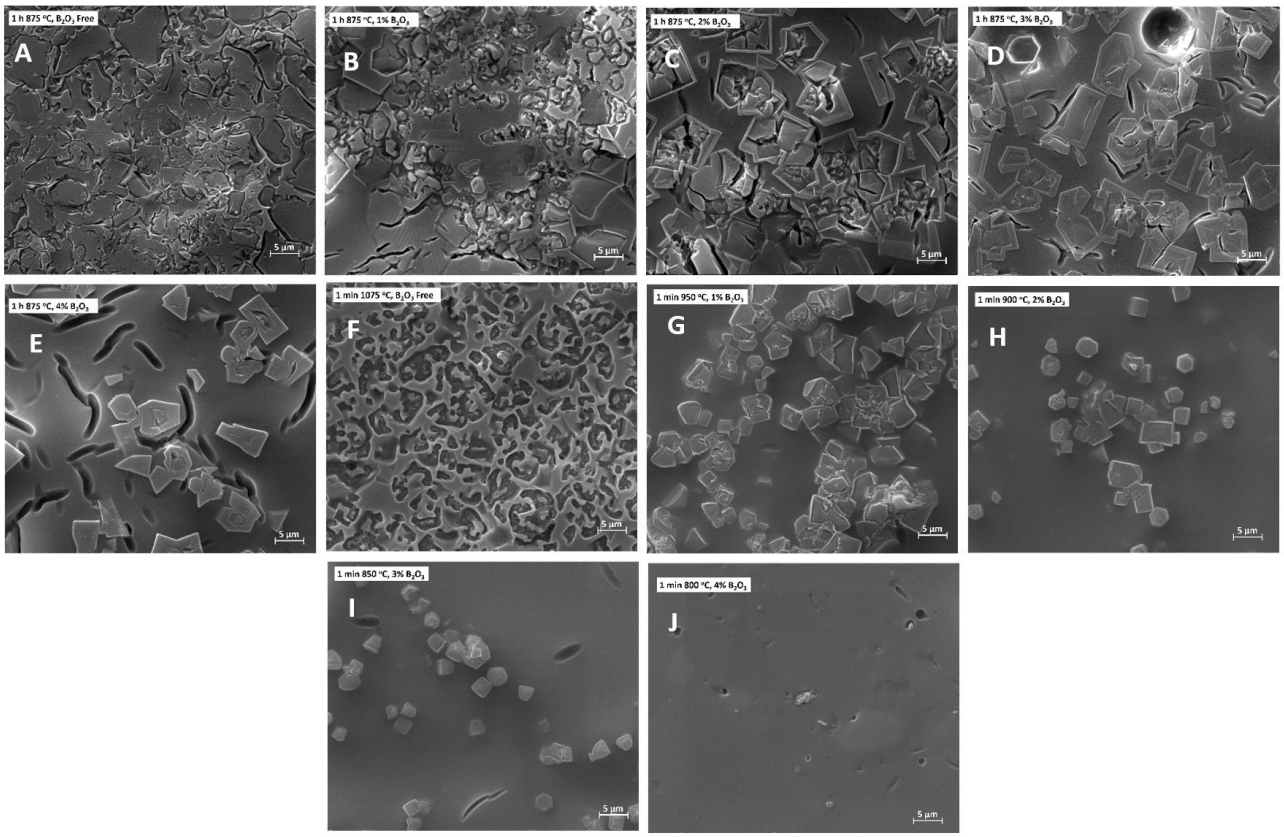

Figure 6. SEM photomicrographs of heat treated glasses at identical temperature 875 °C for 1 h (A-E) and after 1 min hold at the sintering-crystallisation temperatures (F-J) illustrating the decrease in nepheline crystallites content as a result of substituting Al_2O_3 with B_2O_3

SEM micrographs (Fig. 6) show a clear reduction in crystalline phase fraction and crystal size with increasing B_2O_3 content under both heat-treatment schedules. After 1 h at 875 °C, the B_2O_3-free and low-boron glasses exhibit dense, intergrown crystallites forming near-continuous networks, whereas ≥3 mol% B_2O_3 compositions display more isolated and sparsely distributed crystals within a dominant glassy matrix. Under rapid 1 min firing, the boron-free composition develops a high density of fine crystallites, while boron-containing glasses show progressively lower nucleation density and smaller, more widely separated particles, with the 4 mol% B_2O_3 sample remaining largely featureless at this scale. The observed morphologies are consistent with nepheline-type phases and confirm that B_2O_3 suppresses nepheline crystallisation by inhibiting nucleation and growth.

The visual comparison of cylindrical slices (1 h at 875 °C) and rapidly sintered-crystallised discs (1 min firing) in Fig. 7 and Table 3 reveals a strong composition-dependent densification and translucency trend with increasing B_2O_3 content. Lower-boron samples appear more porous and opaque, while ≥2 mol% B_2O_3 samples show reduced porosity and smoother surfaces. At 3–4 mol% B_2O_3, bodies appear dense and well-sintered, although greater shrinkage and slight deformation are observed. Under rapid firing, discs become progressively more translucent with increasing B_2O_3, consistent with reduced crystalline fraction and improved optical homogeneity.

a) b) c) d) e)

Figure 7. Visual comparison of prepared glass-ceramics (cylindrical section slices) with different B_2O_3 contents heat treated at 875 °C for 1 h: a) B_2O_3 free, b) 1% B_2O_3, c) 2% B_2O_3, d) 3% B_2O_3 a) B_2O_3 and e) 4% B_2O_3

Table 3. Visual comparison of glass-ceramics sintered-crystallised at selected temperature for 1 min in dental furnace

Sample Image	Description
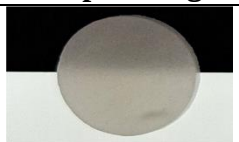	B_2O_3 free, 1 min at 1075 °C- a light-gray, semi-opaque translucent glass-ceramic disc with a smooth surface. Opacity indicates *crystallinity*. Minimal surface scattering suggests fine or sparsely distributed microcrystals.
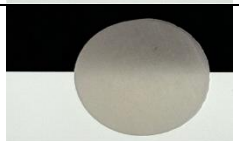	1% B_2O_3, 1 min at 950 °C- a very uniform pale-gray translucent disc with consistent translucency. Optical uniformity indicates a *homogeneous microcrystal distribution* and glassy phase. This sample represent a controlled, mild nucleation stage with limited crystal growth.
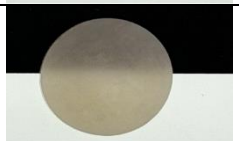	2% B_2O_3, 1 min at 900 °C- a warmer beige-gray translucent disc, slightly darker and more optically dense. Higher absorption/scattering implies *increased glassy* phase.
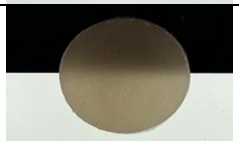	3% B_2O_3, 1 min at 850 °C - a pale-gray disc with mid-range low translucency and smooth polishing. Optical behaviour suggests glassy phases. Slightly more contrast than the 2% sample, but more dense than the 4% sample, consistent with a *SEM observed crystallisation changes.*
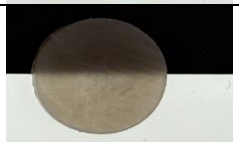	4% B_2O_3, 1 min at 800 °C - a noticeably darker and high translucency glass-ceramic disc with higher optical density. This suggests *glassy phase*, more scattering centres, or altered composition. Could represent porosity.

IV. Conclusions

The present study demonstrates that partial substitution of B_2O_3 for Al_2O_3 in nepheline-based glasses significantly modifies both network structure and crystallisation behaviour, even at low substitution levels. The combined results from DSC, XRD, Raman spectroscopy, dilatometry and SEM establish a consistent structure-property relationship associated with the progressive replacement of tetrahedral AlO_4 units by borate species, predominantly BO_3 groups. XRD and SEM analyses confirm that nepheline crystallisation is strongly inhibited with increasing B_2O_3 content, with near-complete suppression at 4 mol% substitution, while Raman spectra verify that the disruption originates at the atomic scale through borate incorporation and increased non-bridging oxygen character.

The transition from a crystal-bearing glass-ceramics to a predominantly amorphous and thermally stable glass with increasing B_2O_3 highlights the effectiveness of boron as a crystallization inhibitor in aluminosilicate systems. This compositional tunability enables controlled adjustment of microstructure and thermal response, which is particularly valuable for applications requiring translucency, dimensional stability, and resistance to devitrification. From a dental materials perspective, compositions near ~3 mol% B_2O_3 show the most favourable balance of crystallisation resistance, firing stability, and thermal compatibility with zirconia frameworks. Overall, moderate B_2O_3 addition provides an effective strategy for optimising processing reliability and functional performance in nepheline-based glass and glass-ceramic systems and represents a promising glass system for further compositional and processing optimisation.

Acknowledgement: The author would like to acknowledge the Deanship of Graduate Studies and Scientific Research, Taif University for funding this work.

References

1. Y. Jiang, C. Zhang, J. Xu, J. Xu, X.Q. Zhan, N. Ma, F.C. Tsai. “An overview of dental glass–ceramics: From material design to the manufacturing process”, *Int. J. Ceram. Eng. Sci.*, **6** [4] (2024) e10224.
2. S.C. Bayne, “Dental biomaterials: where are we and where are we going?”, *J. Dental Education*, **69** [5] (2005) 571–585.
3. J.R. Kelly, P. Benetti, “Ceramic materials in dentistry: historical evolution and current practice”, *Aust. Dental J.*, **56** (2011) 84–96.
4. A.S. Alzahrani, “Novel ion-exchangeable nepheline glass-ceramics for dental application”, *J. Eur. Ceram. Soc.*, **43** [13] (2023) 15682–15690.
5. A.S. Alzahrani, “Syntheses and characterization of twofold nepheline-combeite glass-ceramics for dental application”, *J. Non-Crystal. Solids*, **596** (2022) 121877.
6. A.S. Alzahrani, “Effect of TiO_2 on the sinter crystallization of nepheline glasses for dental application”, *Int. J. Appl. Glass Sci.*, **13** [4] (2022) 610–619.

7. A.S. Alzahrani, G. Pintori, V.M. Sglavo, "Conventional and electric field-assisted ion exchange on glass-ceramics for dental applications", *J. Eur. Ceram. Soc*., **41** [10] (2021) 5341–5348.
8. E.M. Hamzawy, E.A. El-Meliegy, "Preparation of nepheline glass-ceramics for dental applications", *Mater. Chem. Phys*., **112** [2] (2008) 432–435.
9. W. Moo-Chin, W. Nan-Chung, H. Min-Hsiung, "Preparation of nepheline glass-ceramics and their application as dental porcelain", *Mater. Chem. Phys*., **37** [4] (1994) 370–375.
10. H.R. Guzmán-Carrillo, J.M. Pérez, M. Romero, "Crystallisation of nepheline-based glass frits through fast-firing process", *J. Non-Crystal. Solids*, **470** (2017) 53–60.
11. J. Marcial, J. Crum, O. Neill, J. McCloy, "Nepheline structural and chemical dependence on melt composition", *Am. Mineralog*., **101** [2] (2016) 266–276.
12. A. Shenoy, N. Shenoy, "Dental ceramics: An update", *J. Conserv. Dentistry Endodontics*, **13** [4] (2010) 195–203.
13. L.H. Silva, E.D. Lima, R.B. Miranda, S.S. Favero, U. Lohbauer, P.F. Cesar, "Dental ceramics: A review of new materials and processing methods", *Brazil. Oral Res*., **31** [Supp 1] (2017) e58.
14. K.C. Cheung, B.W. Darvell, "Sintering of dental porcelain: effect of time and temperature on appearance and porosity", *Dental Mater*., **18** [2] (2002) 163–173.
15. P.J. Babu, R.K. Alla, V.R. Alluri, S.R. Datla, A. Konakanchi, "Dental ceramics: Part I - An overview of composition, structure and properties", *Am. J. Mater. Eng. Technol*., **3** [1] (2015) 13–18.
16. W.H. Zachariasen, "The atomic arrangement in glass", *J. Am. Chem. Soc*., **54** [10] (1932) 3841–3851.
17. R.K. Brow, "The structure of simple phosphate glasses", *J. Non-Crystal. Solids*, **263** (2000) 1–28.
18. A. Deshkar, O. Gulbiten, R.E. Youngman, J.C. Mauro, A. Goel, "Why does B_2O_3 suppress nepheline ($NaAlSiO_4$) crystallization in sodium aluminosilicate glasses?", *Phys. Chem. Chem. Phys*., **22** [16] (2020) 8679–8698.
19. F. Chen, G. Wen, H. Yang, P. Tang, Z. Hou, "Formation of nepheline in the heating process of mould fluxes and its effect on sintering behaviour", *Ironmaking Steelmaking*, **51** [4] (2024) 380–393.
20. A. Deshkar, M. Ahmadzadeh, A. Scrimshire, E. Han, P.A. Bingham, D. Guillen, J. McCloy, A. Goel, "Crystallization behavior of iron-and boron-containing nepheline ($Na_2O{\cdot}Al_2O_3{\cdot}2SiO_2$) based model high-level nuclear waste glasses", *J. Am. Ceram. Soc*., **102** [3] (2019) 1101–1121.
21. G.S. Fulcher, "Analysis of recent measurements of the viscosity of glasses", *J. Am. Ceram. Soc*., **75** [5] (1992) 1043–1055.
22. S.T. Rasmussen, W. Ngaji-Okumu, K. Boenke, W.J. O'Brien, "Optimum particle size distribution for reduced sintering shrinkage of a dental porcelain", *Dental Mater*., **13** [1] (1997) 43–50.
23. S.J. Saint-Jean, "Dental glasses and glass-ceramics", pp. 255-277 in *Advanced Ceramics for Dentistry*, Butterworth-Heinemann, 2014.
24. P. Benetti, J.R. Kelly, A. Della Bona, "Analysis of thermal distributions in veneered zirconia and metal restorations during firing", *Dental Mater*., **29** [11] (2013) 1166–1172.
25. D.E. Day, "Mixed alkali glasses - Their properties and uses", *J. Non-Crystal. Solids*, **21** [3] (1976) 343–372.
26. J.O. Isard, "The mixed alkali effect in glass", J. Non-Crystal. Solids, 1 [3] (1969) 235–261.
27. M.S. Bødker, R.E. Youngman, J.C. Mauro, M.M. Smedskjaer, "Mixed alkali effect in silicate glass structure: viewpoint of 29Si nuclear magnetic resonance and statistical mechanics", J. Phys. Chem. B, 124 [45] (2020) 10292–10299.
28. R.H. Doremus, "Mixed-alkali effect and interdiffusion of Na and K ions in glass", *J. Am. Ceram. Soc*., **57** [11] (1974) 478–480.
29. N. Ilie, G. Furtos, "A comparative study of light transmission by various dental restorative materials and the tooth structure", *Operative Dentistry*, **45** [4] (2020) 442–452.
30. A.C. da Silva, A.D. Ribeiro, L.M. Alves, F. de Camargo Ribeiro, T.B. Campos, R.M.de Melo Marinho, "Zirconia gradation and thermal expansion compatibility between infiltration glass and antimicrobial glass", *Ceram. Int*., **48** [14] (2022) 19746–19756.
31. H. Salimkhani, E. Asghari Fesaghandis, S. Salimkhani, B. Abdolalipour, A. Motei Dizaji, T. Joodi, A. Bordbar-Khiabani, "In situ synthesis of leucite-based feldspathic dental porcelain with minor kalsilite and Fe_2O_3 impurities", *Int. J. Appl. Ceram. Technol*., **16** [2] (2019) 552–561.
32. T.F. Whale, M.A. Holden, A.N. Kulak, Y.Y. Kim, F.C. H.K. Meldrum, Christenson, B.J. Murray, "The role of phase separation and related topography in the exceptional ice-nucleating ability of alkali feldspars", *Phys. Chem. Chem. Phys*., **19** [46] (2017) 31186–31193.
33. E.I. Kamitsos, "Infrared studies of borate glasses", *Phys. Chem. Glasses*, **44** [2] (2003) 79–87.
34. D.W. Matson, S.K. Sharma, J.A. Philpotts, "Raman spectra of some tectosilicates and of glasses along the orthoclase-anorthite and nepheline-anorthite joins", *Am. Mineral*., **71** [5-6] (1986) 694–704.
35. R. Oestrike, W.H. Yang, R.J. Kirkpatrick, R.L. Hervig, A. Navrotsky, B. Montez, "High-resolution 23Na, 27Al and 29Si NMR spectroscopy of framework aluminosilicate glasses", *Geochim. Cosmochim Acta*, **51** [8] (1987) 2199–2209.
36. Y. Maruo, G. Nishigawa, M. Irie, K. Yoshihara, T. Matsumoto, S. Minagi, "Does acid etching morphologically and chemically affect lithium disilicate glass ceramic surfaces?", *J. Appl. Biomater. Funct. Mater*., **15** [1] (2017) 93–100.
37. V.F. Reginato, D.T. Kemmoku, R.A. Caldas, A. Bacchi, C.S. Pfeifer, R.L. Consani, "Characterization of residual stresses in veneering ceramics for prostheses with zirconia framework", *Brazil. Dental J*., **29** [4] (2018) 347–353.
38. G. Isgrò, H. Wang, C.J. Kleverlaan, A.J. Feilzer, "The effects of thermal mismatch and fabrication procedures on the deflection of layered all-ceramic discs", *Dental Mater*., **21** [7] (2005) 649–655.
39. R.A. Shahmiri, O.C. Standard, J.N. Hart, C.C. Sorrell, "A review of the characteristics and optimization of optical properties of zirconia ceramics for aesthetic dental restorations", *Int. J. Med. Med. Health Sci.*, **11** [8] (2017) 499–508.